energies

MDPI

Article

Performance Analysis and Comprehensive Evaluation of Solar Organic Rankine Cycle Combined with Transcritical CO_2 Refrigeration Cycle

Na Zhang [1,2], Po Xu [1], Yiming Wang [1], Wencai Tong [3] and Zhao Yang [2,*]

[1] Ginlong Technology Co., Ltd., Ningbo 315712, China; zhangna881127@163.com (N.Z.); damon@ginlong.com (P.X.); jimmy@ginlong.com (Y.W.)
[2] Mechanical Engineering, Tianjin University, Tianjin 300072, China
[3] School of Civil Engineering and Architecture, East China Jiaotong University, Nanchang 330013, China; m18679103264_1@163.com
* Correspondence: zhaoyang@tju.edu.cn

Abstract: In order to achieve efficient utilization of solar energy resources, this study combines the trans-critical organic Rankine cycle (ORC) power cycle (TORC) with the trans-critical CO_2 refrigeration cycle (TCO_2). Additionally, a comprehensive three-level index decision evaluation system is developed based on system safety and environmental protection, thermodynamics, and techno-economic performance. The evaluation focuses on typical medium- and high-temperature solar energy applications and considers six organic working gases. The evaluation results demonstrate that the R600 + CO_2 solution outperformed the others. This solution achieved a maximum net output power (P_{net}) of 1531.31 kW and 2306.43 kW, a maximum coefficient of performance (COP) of 3.16, a predicted payback period of 2.651 years and 2.033 years, and a benefit–investment ratio of 4.533 and 5.773.

Keywords: solar energy; trans-critical ORC; trans-critical CO_2; fuzzy decision-making; integrated evaluation

Citation: Zhang, N.; Xu, P.; Wang, Y.; Tong, W.; Yang, Z. Performance Analysis and Comprehensive Evaluation of Solar Organic Rankine Cycle Combined with Transcritical CO_2 Refrigeration Cycle. *Energies* **2023**, *16*, 5557. https://doi.org/10.3390/en16145557

Academic Editor: Wen Su

Received: 30 May 2023
Revised: 4 July 2023
Accepted: 17 July 2023
Published: 22 July 2023

1. Introduction

With the rapid development of the economy and society, accompanied by an increasing intensity of human activity, the emission of greenhouse gases such as carbon dioxide has accelerated, resulting in more severe phenomena known as global warming and glacial melting. Global energy consumption has been rising sharply, exerting a continuous influence on human beings and giving rise to issues like air pollution, energy conservation, and emissions reduction. In response to this crisis, countries worldwide are actively engaged in research into and the development of new renewable energy sources [1]. When compared to other emerging energy sources like nuclear power, wind power, and hydropower, solar energy utilization offers the advantage of being geographically unrestricted, allowing for local development and utilization in any region. With an abundant supply that can serve humanity for billions of years, solar energy causes no environmental pollution and does not disrupt the ecological balance. As of the end of 2022, China's cumulative installed capacity for solar thermal power generation reached 588 MW, accounting for 8.3% of the global cumulative installed capacity for solar thermal power generation [2], signifying its tremendous potential for development. From an energy conversion perspective, the utilization of solar thermal power generation technology enables the conversion of low-grade energy (heat energy) to high-grade energy (electric energy). Additionally, this system operates with minimal irreversible losses and exhibits high energy conversion efficiency, leading to significant social, environmental, and economic benefits.

The ORC Is currently the preferred technology for utilizing medium- and low-temperature heat sources, including solar energy, gas waste heat, and biomass sources [3].

The ORC system converts low-grade heat energy into high-grade electric energy output, providing advantages in resource conservation, carbon emissions reduction, ecological benefits, and improved power generation performance. Currently, research in the field of ORC systems primarily focuses on two aspects: working fluid selection and system optimization. Regarding the selection of working fluids for ORC systems, Shahverdi [4] developed an energy collection system that integrates the Archimedean spiral turbine with solar ORC and examined the impact of various working fluids, such as R134a, R245ca, and R245fa, on system performance. Feng [5] chose R123, R245fa, R600, R601, and R601a as working fluids for ORC systems and conducted an analysis of how operating parameters affect the system's thermal performance. The research findings demonstrated that R123fa exhibited the highest thermal efficiency and exergy efficiency, whereas R245fa had the greatest overall irreversibility losses. Furthermore, Shalaby [6] developed a simulation model for a 1 kW solar ORC, employing a trough-type collector to heat the working fluid. By varying parameters such as the evaporation temperature, pressure, and flow rate, the performance of five working fluids was compared and analyzed. The results indicated that isopentane achieved the highest performance with a thermal efficiency of 15.5% at an evaporation temperature of 173 °C, an evaporation pressure of 11.5 bar, and a flow rate of 36 kg/h. Concerning the optimization of ORC systems, Li [7] investigated the impact of a narrow temperature difference at the evaporation temperature on the system, with a specific focus on subcritical ORC and the optimization objective of minimizing production cost. The research findings offered the optimal evaporation temperature for subcritical ORC at various heat source temperatures, the temperature difference between the evaporator and condenser, and the condensation temperature, which minimizes power generation costs. The study highlighted that the working fluids corresponding to the critical temperature range of 180–210 °C exhibited optimal thermoeconomic performance for the ORC system. Additionally, Bufi [8] aimed to maximize the thermal efficiency of the ORC cycle and performed single-objective optimization for toluene and R113, two working fluids. They employed a non-dominated sorting genetic algorithm to conduct multi-objective optimization for the fluid with the optimal performance, evaluating cycle parameters that would maximize thermal efficiency while minimizing heat exchanger surface area.

Similar to the development of the ORC, trans-critical CO_2 refrigeration cycle technology has garnered increasing attention due to its clean, efficient, and environmentally friendly attributes. Additionally, CO_2 as a refrigerant offers advantages including high density, low viscosity, minimal flow loss, and excellent heat transfer capabilities. However, the high critical pressure of CO_2 imposes stricter requirements on materials and manufacturing processes, and there is still room for improvement in compression technology [9]. Due to the ORC system's capability of utilizing low-grade thermal energy for power generation and the cross-critical CO_2 refrigeration cycle's ability to provide refrigeration with minimal compression work, they can be combined to create a thermally driven refrigeration cycle. This innovative technology was initially proposed by Prigmore [10], who employed solar energy to drive an ORC system for vapor compression refrigeration. Subsequently, scholars have extensively researched this integrated system. Jeong [11] conducted a comprehensive investigation into the operational characteristics of refrigeration cycles driven by the organic Rankine cycle, comparing three candidate working fluids: R123, R134a, and R245ca. The system's maximum COP was found to be 1.75, with R123 identified as the optimal working fluid. Aphornratana [12] focused on studying the influence of evaporating and condensing temperatures on the performance of the Rankine vapor compression refrigeration system. Furthermore, Wu [13] effectively combined an ORC system, which utilized a building surface solar energy collection system as a heat source, with a refrigeration cycle system for building cooling. Under optimal operating conditions, the unit cooling cost of this integrated system was determined to be 0.24 USD·(kW·h)$^{-1}$.

Based on the aforementioned points, it is evident that such studies mainly focus on analyzing the thermodynamic performance and the second law of thermodynamics. Such studies primarily address the system's thermodynamic performance and techno-economic

evaluation, and optimize working fluids and target parameters. However, practical applications often focus solely on single-level indicators, such as thermodynamic performance, neglecting to consider the influence of other levels of evaluation criteria, such as techno-economic performance and socio-environmental benefits, on the overall system performance. Moreover, the inherent interconnections between different evaluation indicators are often overlooked, thus rendering the planned optimal solution unable to achieve the desired benefits. Therefore, it is crucial to seek the establishment of a comprehensive evaluation system for solar ORC combined with trans-critical CO_2 refrigeration cycles considering multiple indicators. The development of reliable and effective decision-making methods for system planning is of great importance in actively promoting the efficient development of the solar energy industry and improving the utilization of solar energy resources.

This paper aims to enhance the overall efficiency of utilizing solar energy resources by focusing on medium- to high-temperature solar energy (100–200 °C). It employs a trans-critical organic Rankine cycle power cycle to drive a trans-critical CO_2 refrigeration cycle. A three-level comprehensive decision evaluation system is constructed for the combined solar TORC and TCO_2 system based on a fuzzy decision-making algorithm. The system enhances the analysis of single-objective parameters and considers the interplay of indicators across different levels. The study conducts a thorough quantitative evaluation of the overall performance of the combined system. It enables a direct comparison of system scheme benefits and drawbacks, providing investors with a comprehensive perspective during the pre-design phase. This approach facilitates decision-making based on actual requirements, consequently enhancing the system's operational efficiency.

2. System Description

Figures 1 and 2 illustrate the operational principles and T-s (temperature–entropy) diagram of the combined solar TORC and TCO_2 system. The TORC power cycle follows the sequential process of 1–2–3–4–5, whereas the TCO_2 refrigeration cycle proceeds through the process of 6–7–8–9. The state points denoted as g_{win}–g_{wout} represent the heat exchange process involving the transfer of thermal energy in evaporator 1 using a heat transfer oil. Similarly, the state points labeled A_{irin}–A_{irout} denote the cooling process of the air within evaporator 2. Furthermore, the state points indicated as C_{win}–C_{wout} represent the heat absorption process by the cooling water within the condenser. Within the TORC system, the turbine plays a dual role of generating power and driving the compressor of the TCO_2 system through a coupling device.

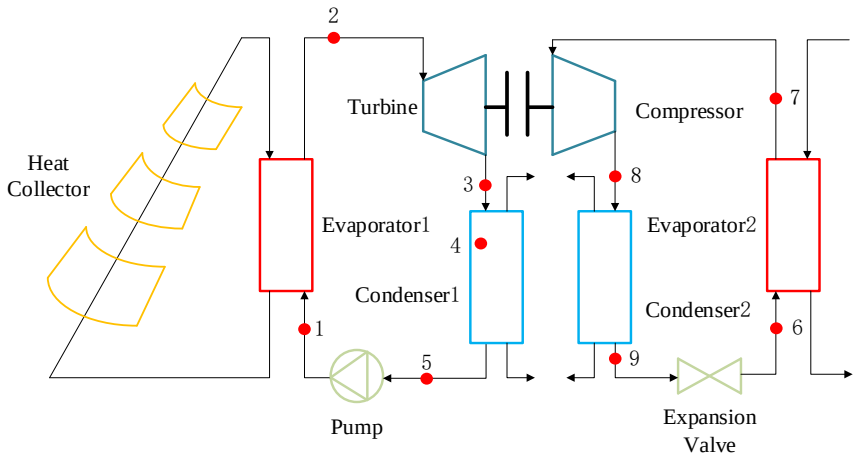

Figure 1. Schematic diagram of combined solar TORC and TCO_2 system.

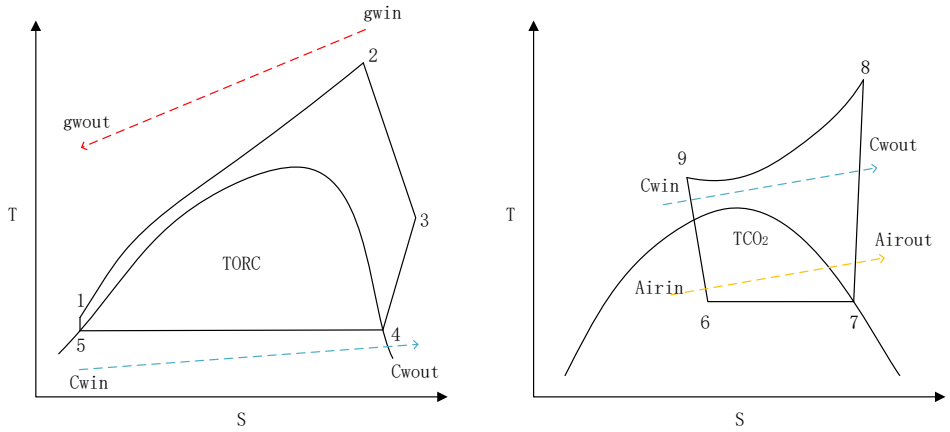

Figure 2. T-s diagram of combined solar TORC and TCO_2 system.

In addition, the heat collector belongs to the spectral sail thermal mediation vacuum tube collector (116 tubes/group; each tube has a collection power of 60 W; the total collection power is about 14 kW) for system research. According to the light intensity of the cities and the annual light intensity distribution, we assumed that the light intensity of the system was 500 W/m^2 and the solar heat collection efficiency was 45%.

The combined solar TORC and TCO_2 system operates under the following assumptions:

(1) The entire system operates in a stable state.
(2) Pressure drops and heat losses within the system are neglected.
(3) The output power of the turbine is fully employed to drive the operation of the compressor.

3. Workpiece Selection

In this paper, the Matlab software was utilized to access the NIST (National Institute of Standards and Technology) Refprop database for the purpose of investigation. Six organic working fluids were selected as initial candidates for the combined solar TORC and TCO_2 system, based on indicators such as safety level, ALT (atmospheric lifetime), ODP (ozone depletion potential), and GWP (global warming potential). Table 1 presents the thermodynamic and environmental properties of the six selected organic working fluids.

Table 1. Working fluid properties in combined solar TORC and TCO_2 system [14–17].

	Critical Temperature/°C	Critical Pressure/MPa	Safety Level	ALT/Year	ODP	GWP
R134a	101.06	4.0593	A1	13.4	0	1430
R1270	91.061	4.555	A3	0.001	0	1.8
R142b	137.11	4.055	A2	17.2	0.065	2310
R227ea	101.75	2.925	A1	38.9	0	3320
R600	151.975	3.796	A3	0.02	0	20
R600a	134.66	3.629	A3	0.016	0	20

4. Computational Modeling

Table 2 presents the thermal source conditions utilized in the computation, along with the diverse operational parameters necessary for system calculations.

Table 2. Operating conditions of combined solar TORC and TCO_2 system.

Parameters	Value
Collector temperature, T_{gwin} (°C)	182.23
Heat transfer oil	YD-320
Heat transfer oil density	0.85–0.88
Heat transfer oil specific heat capacity kJ/(kg.K)	2.5
Heat transfer oil flow rate, mgw (kg/s)	13.64
Condensing temperature, T_{cond} (°C)	35
Evaporator 1 narrow point temperature difference, $T_{pinch\text{-}e1}$ (°C)	10
Condenser 1 narrow point temperature difference, $T_{pinch\text{-}c1}$ (°C)	5
Evaporator 2 narrow point temperature difference, $T_{pinch\text{-}e2}$ (°C)	5
Condenser 2 narrow point temperature difference, $T_{pinch\text{-}c2}$ (°C)	5
TORC $_{turbine}$ isentropic efficiency, $\eta_{turbine}$	0.75
Isentropic efficiency of the TORC workhorse pump, η_{pump}	0.7
TCO_2 compressor isentropic efficiency, η_{comp}	0.9
Cooling water inlet temperature, T_{cwin} (°C)	20
Air inlet temperature, T_{airin} (°C)	20
Ambient temperature, T_0 (°C)	20
Ambient pressure, P_0 (MPa)	0.101

Based on the first and second laws of thermodynamics, the following formulas were introduced to calculate the thermodynamic evaluation indices of the combined solar TORC and TCO_2 system [18]. The thermodynamic calculation models of the main components of the system are shown in Table 3.

Table 3. Thermodynamic analysis of combined TORC and TCO_2 system [19,20].

	First Law of Thermodynamics	Second Law of Thermodynamics
Evaporator 1	$Q_{evaporator1} = m_{wf}(h_2 - h_1)$	$I_{evaporator1} = \left(E_{gwin} + E_1\right) - (E_{gwout} + E_2)$
Condenser 1	$Q_{condenser1} = m_{wf}(h_3 - h_5)$	$I_{condenser1} = (E_{cwin} + E_3) - (E_{cwout} + E_5)$
Pump	$P_{pump} = m_{wf}(h_1 - h_5)$	$I_{pump} = m_{wf}T_0(s_1 - s_5)$
Turbine	$P_{turbine} = m_{wf}(h_2 - h_3)$	$I_{turbine} = m_{wf}T_0(s_3 - s_2)$
Evaporator 2	$Q_{evaporator2} = m_{CO_2}(h_7 - h_6)$	$I_{evaporator2} = Q_{evaporator2}\left(1 - \frac{T_0}{T_{eva2}}\right) + E_6 - E_7$
Condenser 2	$Q_{condenser2} = m_{CO_2}(h_8 - h_9)$	$I_{condenser2} = (E_8 - E_9) + (E_{cwin} - E_{cwout})$
Compressor	$P_{comp} = P_{net} = m_{CO_2}(h_8 - h_7)$	$I_{comp} = m_{CO_2}T_0(s_8 - s_7)$
Expansion valve	$h_9 = h_6$	$I_{exv} = m_{CO_2}T_0(s_6 - s_9)$

The net output power of the TORC system:

$$P_{net} = P_{turbine} - P_{pump} \tag{1}$$

The thermal efficiency of the TORC system:

$$\eta_{t-TORC} = P_{net}/Q_{evaporator1} \cdot 100 \tag{2}$$

The exergy of each state point:

$$E_i = m[(h_i - h_0) - T_0(s_i - s_0)] \tag{3}$$

where m denotes the mass flow rate, s_i represents the entropy of the state points (i = 1 … 7), and the subscript 0 indicates the ambient condition.

The exergy losses caused by cooling water flowing out:

$$I_{out}^{cooling\ water} = E_{cwout} - E_{cwin} \tag{4}$$

The total exergy losses of the TORC system:

$$I_{TORC} = I_{pump} + I_{evaporator1} + I_{turbine} + I_{condenser1} + I_{out}^{cooling\,water} \quad (5)$$

The net exergy of the heat-conducting oil flowing into the system:

$$E_{gw} = P_{net} + I_{TORC} \quad (6)$$

The exergy efficiency of the TORC system:

$$\eta_{e-TORC} = P_{net}/E_{gw} \quad (7)$$

where the subscripts *in* and *out* indicate the inlet and outlet states of the target fluid, respectively.

The cooling coefficient of the performance of the TCO_2 system:

$$COP = Q_{evaporator2}/P_{comp} = Q_{evaporator2}/P_{net} \quad (8)$$

The exergy efficiency of the TCO_2 system:

$$\eta_{e-TCO_2} = Q_{evaporator2}(T_{cond2}/T_{eva2} - 1)/P_{comp} \times 100 \quad (9)$$

The exergy efficiency of the combined TORC and TCO_2 system:

$$\eta_e = Q_{evaporator2}(T_{cond2}/T_{eva2} - 1)/(E_{gw} + P_{pump}) \times 100 \quad (10)$$

where $T_{eva2} = (T_{air_{out}} - T_{air_{in}})/\ln(T_{air_{out}}/T_{air_{in}})$, $T_{cond2} = (T_{cw_{out}} - T_{cw_{in}})/\ln(T_{cw_{out}}/T_{cw_{in}})$;

Techno-economic evaluation indexes were measured as shown in Table 4 [21,22].

Table 4. Techno-economic analysis of combined TORC and TCO_2 system.

Indicators	Formula
ARC	$ARC = (A_{evaporator2} + A_{condenser2})/Q_{evaporator2}$
$Cost_{2019}$	$Cost_{2001} = C_{BM,pump} + C_{BM,evaporator1} + C_{BM,turbine} + C_{BM,condenser1} + C_{BM,comp} + C_{BM,condenser2} + C_{BM,exv} + C_{BM,evaporator2}$ $Cost_{2019} = Cost_{2001} CEPCI_{2019}/CEPCI_{2001}$
RPC	$RPC = (Cost_{2019} CRF + f_k Cost_{2019})/\left(Q_{evaporator2} h_{working-time}\right)$ $CRF = i(1+i)^{time}/\left((1+i)^{time} - 1\right)$
DPP	$DPP = -\ln(1 - kCost_{2019}/F_{n0})/\ln(1+k)$ $F_{n0} = E_P\left(Q_{evaporator2} h_{working-time}\right) - f_k Cost_{2019}$
SIR	$SIR = B_{time}/C_{time}$ $B_{time} = \sum_{j=1}^{time}\left(Q_{evaporator2} h_{working-time} E_p (1+r)^j/(1+i)^j\right)$ $C_{time} = \sum_{j=0}^{time}\left((f_k Cost_{2019})(1+r)^j/(1+i)^j\right)$

In Table 4, $CEPCI$ is the chemical cost index, where $CEPCI_{2001} = 397$ and $CEPCI_{2019} = 607.5$ [23]; the cost of the expansion valve in the TCO_2 system is 15% of the cost of the compressor, condenser 2, and evaporator 2 [24,25]; CRF is the capital recovery factor; f_k is the operation and maintenance cost factor, set at 1.65%; $h_{working-time}$ is the annual operating time of the system, set at 8100 h; i is the annual interest rate, set at 5%; $time$ is the system evaluation time, set at 15 years; k is the system depreciation rate, set at 0.05; F_{n0} is the net present value of the system revenue; E_P is the selling price per unit

of cooling capacity, set at USD 0.1/(kW-h) [26]; B_{time} and C_{time} are the net present value of total revenue and total investment during the evaluation period, respectively, where $j = 1 \ldots 15$; and r is the inflation rate, set at 2.9%.

Based on the described evaluation indicators, a comprehensive decision evaluation system was constructed for the combined solar TORC and TCO_2 system, comprising three levels of indicators.

The first level consists of physical evaluation indices: the safety level, ALT, ODP, and GWP.

The second level comprises thermodynamic evaluation indices: the COP of the TCO_2 system, η_{t-TORC} and η_e.

The third level includes technical and economic evaluation indices: ARC, $Cost_{2019}$, RPC, DPP, and SIR.

The three-level indicator fuzzy decision is calculated by the following equation [27]:

$$\boldsymbol{B_i} = \boldsymbol{W_i} \times \boldsymbol{R_i} \tag{11}$$

where $\boldsymbol{R_i}$ denotes the system scheme weight matrix, $\boldsymbol{W_i}$ denotes the system hierarchy index weight matrix, and $\boldsymbol{B_i}$ denotes the system decision evaluation matrix.

5. Results and Discussion

Figure 3 illustrates the variation of the COP with the condensing pressure (P_8) and evaporating temperature (T_7) in the combined solar TORC and TCO_2 system. The evaporating temperature (T_7) in evaporator 2 ranged from 248.15 K to 273.15 K, whereas the condensing pressure (P_8) in condenser 2 ranged from 8.4 MPa to 10.0 Mpa. The post-condensing temperature (T_9) in CO_2 remained fixed at 308.15 K. The system COP represents the ratio of heat absorption to compressor power consumption in evaporator 2, where the compressor is coupled to the turbine. It is important to note that the coupling exhibited no mechanical transmission losses, and the turbine's output work could be entirely utilized to drive the compressor. Under these operating conditions, the TORC system reached its maximum P_{net}.

The results indicate a trend in the COP of the system whereby it initially increased and subsequently decreased, with an increase in cdondensing pressure given a constant evaporation temperature. Conversely, when the condensing pressure remained constant, the COP of the system increased with an increase in evaporation temperature. The COP is derived from the ratio of the enthalpy difference between the evaporation process (state points 6–7) and the compression process (state points 7–8), expressed as $(h_7 - h_6)/(h_8 - h_7) = \Delta h_{7-6}/\Delta h_{8-7}$. Under constant evaporation temperature conditions, Δh_{7-6} and Δh_{8-7} both increased with the increase in condensing pressure, with the magnitude of increase being consistently maintained. At lower condensing pressures, the increase in Δh_{7-6} was obvious, and then the increase decreased with the increase in condensing pressure, which made the COP increase and then decrease with the increase in condensing pressure in general. When the condensing pressure remained constant, Δh_{7-6} increased and then decreased with the increase in evaporating temperature, Δh_{8-7} decreased with the increase in evaporating temperature, and the decrease in Δh_{8-7} was always larger than that of Δh_{7-6}. Consequently, the COP displayed a gradual increase with an increase in evaporating temperature.

In addition, Figure 3 demonstrates that the COP values of the TCO_2 system remained constant for different organic working materials, even when the condensing pressure (P_8) and evaporating temperature (T_7) varied within the same range. This observation indicates that although the configuration and operating conditions of the TCO_2 system were fixed, altering the circulating working materials in the TORC system did not affect the COP of the combined solar TORC and TCO_2 system. It is important to note that different P_{net} could still be obtained. The COP of the system reached its maximum value of 3.162 at P_8 = 8.8 MPa and T_7 = 273.15 K throughout the entire variation interval between T_7 and P_8.

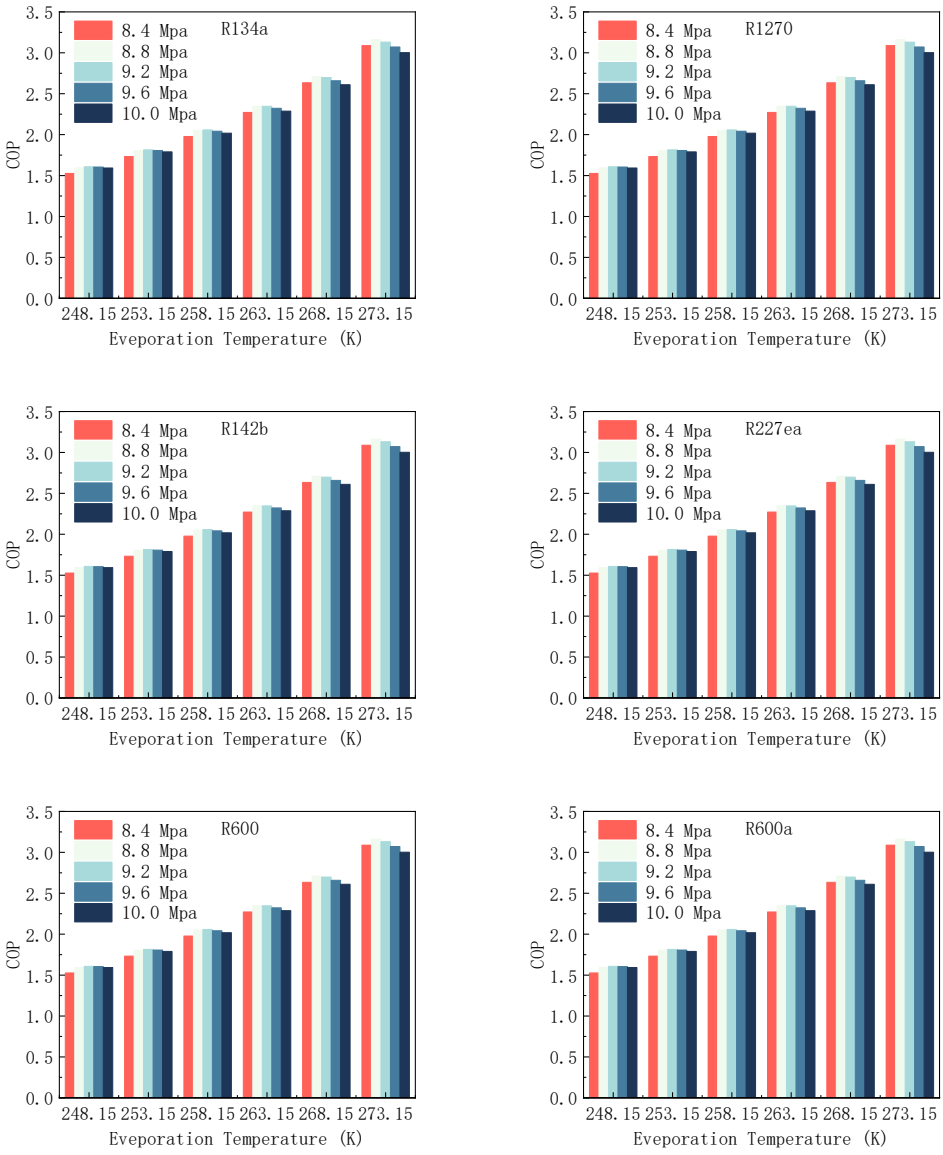

Figure 3. Variation of COP for combined solar TORC and TCO_2 system.

Figure 4 illustrates the changes in η_e within the combined TORC and TCO_2 system, concerning variations in condensing pressure (P_8) and evaporating temperature (T_7). The operational parameters aligned with the analysis conducted in the COP section. Exergy represents the maximum usable work of the system, whereas exergy efficiency indicates the extent to which exergy is effectively utilized within the system. It is defined as the ratio of the net output work to the net exergy input of the system. A higher exergy efficiency indicates increased exergy utilization within the system.

From Figure 4, it can be seen that the system η_e increased with increasing condensing pressure and evaporating temperature. For each organic mass, the sum of the solar energy entering the chamber and the work consumed by the mass pump $E_{gw} + P_{pump}$ was a constant value. When the evaporation temperature was fixed, T_{cond2}/T_{eva2} tended to decrease and then increase with the increase in condensing pressure, $Q_{evaporator2}$ showed an increasing trend, and the product of the two increased with the increase in condensing pressure. When the condensing pressure was fixed, T_{cond2}/T_{eva2} decreased with the increase in evaporation temperature, $Q_{evaporator2}$ still showed a gradual increase, and the latter changed more than the former, resulting in an increase in their product with the increase in evaporation temperature.

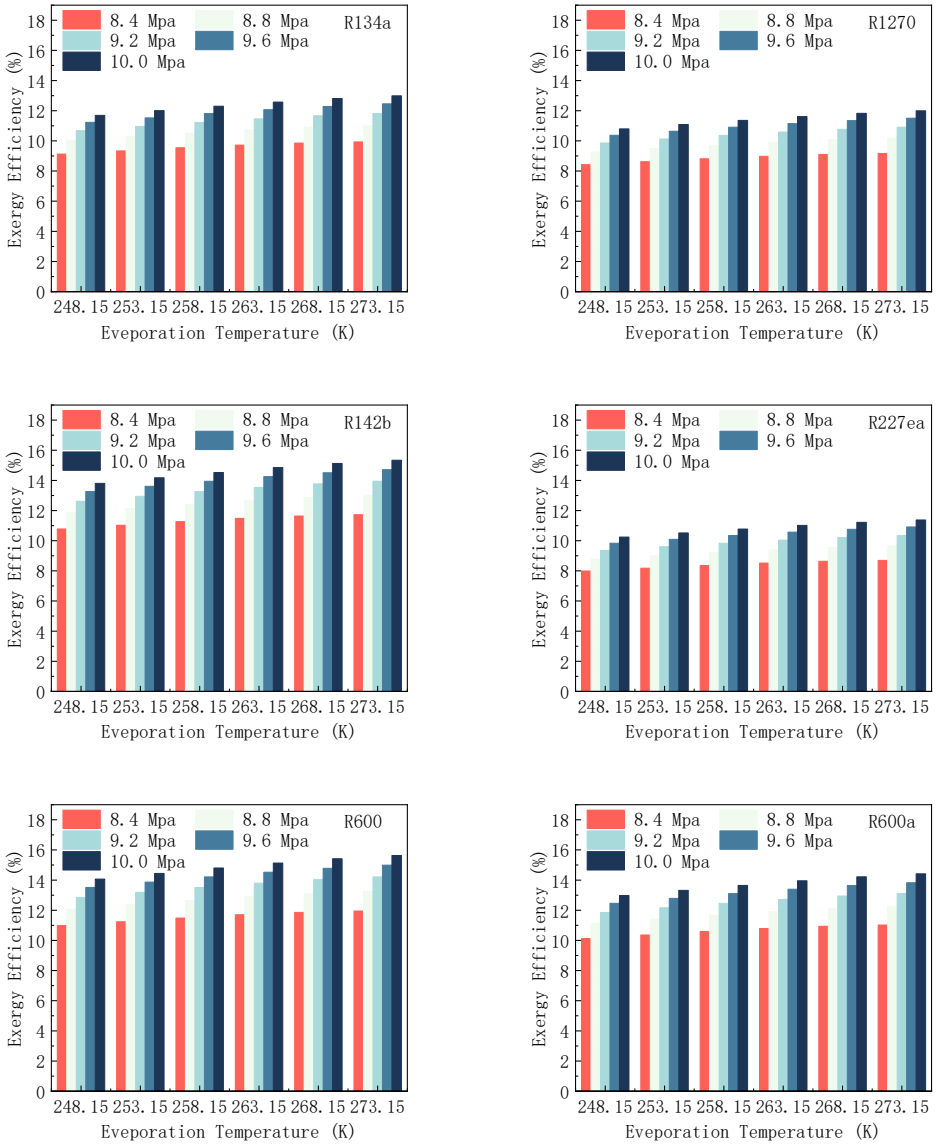

Figure 4. Variation of exergy efficiency for combined solar TORC and TCO_2 system.

For various organic working fluids, the combined solar TORC (R600) and TCO_2 system reached the highest value of 15.63% at P_8 = 8.8 MPa and T_7 = 273.15 K.

Figure 5 illustrates the relationship between the ARC and the condensing pressure (P_8) and evaporating temperature (T_7) in the combined solar TORC and TCO_2 system. The system's ARC represents the ratio of the evaporator 2 and condenser 2 areas to the cooling capacity. A smaller ARC signified a more compact system and better system economics. In the combined solar TORC and TCO_2 system, both the heat exchanger area and cooling capacity increased with the condensing pressure and evaporating temperature. In the combined solar TORC and TCO_2 system, both the heat exchanger area and the cooling capacity increased with the condensing pressure and the evaporating temperature. When the evaporating temperature was certain and at a lower condensing pressure, the increase in the heat exchanger area was smaller than the cooling capacity, and as the condensing pressure increased, the heat exchanger area increased gradually more than the cooling capacity, making the system ARC increase with the condensing pressure first decrease and then increase. When the condensing pressure was certain, the evaporation temperature increased, and the system ARC with the evaporation temperature increased and decreased, the reason being that the heat exchanger area's rising trend was always smaller than the refrigeration capacity. For various organic working fluids, the combined solar TORC (R600)

and TCO_2 system had the lowest ARC of 0.0817 (m^2/kW), corresponding to working points of P_8 = 8.8 MPa and T_7 = 273.15 K.

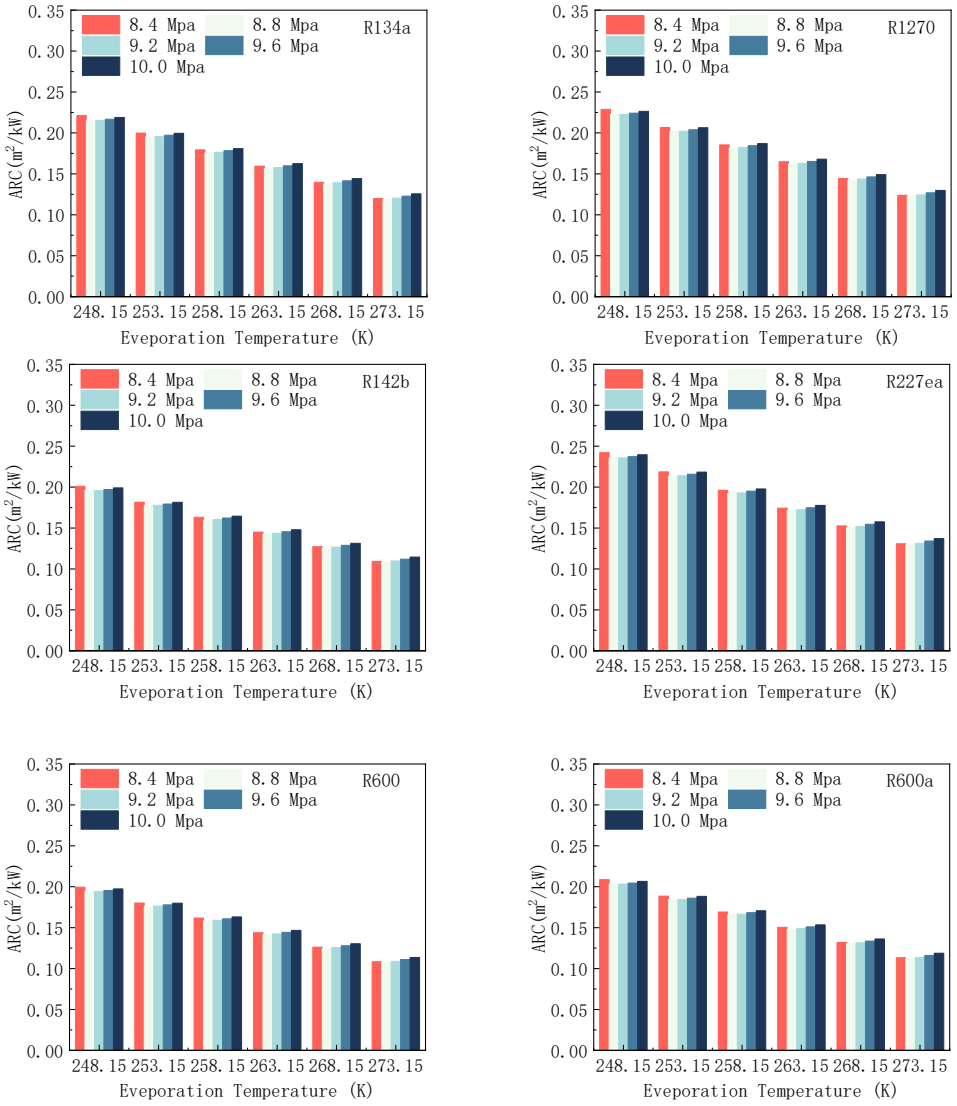

Figure 5. Variation of ARC for combined solar TORC and TCO_2 system.

By utilizing the maximum values of P_{net} and COP as the objective function in the combined solar TORC and TCO_2 system, the remaining evaluation indexes could be determined under the corresponding operating conditions at P_8 = 8.8 MPa and T_7 = 273.15 K. These values aligned with the results presented in Table 5.

Table 5. Simulated optimal results of combined TORC and TCO_2 system.

Rank	COP	η_e/%	ARC(m^2/kW)	RPC (USD/(kW-h))	Total-$Cost_{2019}$ (USD 105)	DPP	SIR
D1	3.16	11.02	0.119	0.029	87.48	2.98	4.08
D2		10.17	0.123	0.03	86.11	3.09	3.95
D3		13.01	0.108	0.027	91.76	2.695	4.46
D4		9.65	0.13	0.032	83.13	3.257	3.77
D5		13.26	0.107	0.026	91.49	2.651	4.53
D6		12.23	0.112	0.028	89.65	2.788	4.33

Subsequently, the three-level fuzzy decision evaluation of each indicator could be conducted. The combined solar TORC and TCO_2 system consists of six programs, namely,

R134a + CO_2 (D1), R1270 + CO_2 (D2), R142b + CO_2 (D3), R227ea + CO_2 (D4), R600 + CO_2 (D5), and R600a + CO_2 (D6).

The tier indicators are assigned numerical values representing different parameters. These parameters include safety level (C1), atmospheric lifetime (C2), ozone depletion potential (C3), global warming potential (C4), TORC system thermal efficiency (C5), TCO_2 system cooling coefficient of performance (C6), combined system exergy efficiency (C7), heat transfer area per cooling capacity (C8), cost per cooling capacity (C9), total cost (C10), depreciated payback period (C11), and system-to-investment ratio (C12). The modifications aim to enhance clarity and concision by rephrasing the sentence and providing clearer explanations for each parameter.

When calculating the weight matrix for the scheme, smaller values of C1, C2, C3, C4, C8, C9, C10, and C11 are considered better. When comparing the values of small indicators across different programs, a small value is assigned a score of 1, whereas a large value is assigned a score of 0. For large indicators such as C5, C6, C7, and C12, larger values are considered better. When comparing large indicators across different programs, small values are assigned a score of 0, whereas large values are assigned a score of 1. After calculating the total scores of indicators for each program, they are ranked in descending order and weights. The weight interval for program indicators is considered 0.5.

It is necessary to rank hierarchical indicators according to their importance when calculating the hierarchical indicator weight matrix. The importance of the first-tier indicators is as follows: C3 > C4 > C2 > C1. The importance of the second-tier indicators is as follows: C7 > C6 > C5. The importance of the third-tier indicators is as follows: C9 > C12 > C11 > C10 > C8.

After multiplying the weight matrix of the first-level scheme by the weight matrix of the first-level indicators, the resulting first-level decision evaluation should be placed in the last column of the second-level scheme weight matrix. Subsequently, the weight matrix of the second-level indicators should be multiplied by the weight distribution coefficient 3/(3 + 1), and the value 1/(3 + 1) should be placed in the last column of the second-level indicator weight matrix. Finally, the second-level scheme weight matrix should be multiplied by the second-level indicator weight matrix to obtain the second-level decision evaluation results. The procedure for the third level is identical to that of the second level, except that 3/(3 + 1) should be replaced with 5/(5 + 1) and 1/(3 + 1) with 1/(5 + 1). The results of the comprehensive decision evaluation for all three levels of indicators can be found in Table 6.

Table 6. Three-level fuzzy decision results of combined TORC and TCO_2 system.

	D1	D2	D3	D4	D5	D6
Tier 1 evaluation results	0.135	0.172	0.090	0.114	0.129	0.137
Tier 1 evaluation ranking	3	1	7	6	5	2
Tier 2 evaluation results	0.129	0.114	0.151	0.089	0.182	0.145
Second-tier evaluation ranking	4	6	2	7	1	3
Tier 3 evaluation results	0.124	0.097	0.164	0.084	0.202	0.144

The integrated decision evaluation of the three levels of indicators for the combined solar TORC and TCO_2 system yielded the following results: R600 + CO_2 > R142b + CO_2 > R600a + CO_2 > R134a + CO_2 > R1270 + CO_2 > R227ea + CO_2. Based on these results, it is evident that the R600 + CO_2 scheme outperformed others in the medium- and low-temperature combined solar TORC and TCO_2 system.

6. Conclusions

This paper is based on the established combined solar TORC and TCO_2 system. It presents models for evaluating working fluid properties, thermodynamics, technical and economic aspects, heat transfer, and fuzzy decision-making. The system operation is simulated iteratively, and analysis is conducted using the maximum P_{net} and the maximum

COP as objective functions. By combining the evaluation values of various indicators for the system's optimal operating conditions, a comprehensive decision evaluation is performed. The study provides intuitive rankings of the advantages and disadvantages among different system schemes, which are of significant guidance in exploring the following:

(1) In the combined solar TORC and TCO_2 system, the optimal scheme was R600 + CO_2. It achieved a maximum net output power of 1531.31 kW and a maximum COP of 3.16 under the conditions P_2 = 4.5 MPa, T_2 = 445 K, P_8 = 8.8 MPa, and T_7 = 273.15 K.

(2) In the combined solar TORC and TCO_2 system, the comprehensive decision evaluation based on the three-level index ranked the schemes as follows:

R600 + CO_2 > R142b + CO_2 > R600a + CO_2 > R134a + CO_2 > R1270 + CO_2 > R227ea + CO_2.

In conclusion, the evaluation model of the combined solar TORC and TCO_2 system, along with the comprehensive decision evaluation system based on the three-level index, considers the inherent connections between various schemes and level indicators. Decision-makers can adjust the weights of the indicators based on specific requirements to develop operational strategies and solutions. This process can offer initial design concepts for the combined solar TORC and TCO_2 system.

Author Contributions: Conceptualization, N.Z.; Methodology, N.Z.; Software, N.Z.; Validation, P.X.; Formal analysis, P.X.; Investigation, P.X.; Resources, Y.W.; Data curation, Y.W. and W.T.; Writing—original draft, Y.W.; Writing—review & editing, Z.Y.; Visualization, W.T.; Project administration, Z.Y. All authors have read and agreed to the published version of the manuscript.

Funding: This research received no external funding.

Data Availability Statement: The data that support the findings of this study are available from the corresponding author upon reasonable request.

Conflicts of Interest: The authors declare no conflict of interest.

References

1. BP. BP World Energy Outlook. 2023. Available online: https://www.bp.com/en/global/corporate/energy-economics/energy-outlook.html?_ga=2.59297197.1009417931.1689672254-825680902.1689672254 (accessed on 10 June 2023.).
2. National Development and Reform Commission. *Renewable Energy Development Plan for the 14th Five-Year Plan*; National Energy Administration: Beijing, China, 2022.
3. Pei, G.; Li, J.; Ji, J. Analysis of low temperature solar thermal electric generation using regenerative organic Rankine cycle. *Appl. Therm. Eng.* **2010**, *30*, 998–1004. [CrossRef]
4. Shahverdi, K.; Loni, R.; Ghobadian, B.; Monem, M.J.; Gohari, S.; Marofi, S.; Najafi, G. Energy harvesting using solar ORC system and Archimedes Screw Turbine (AST) combination with different refrigerant working fluids. *Energy Convers. Manag.* **2019**, *187*, 205–220. [CrossRef]
5. Feng, J.S.; Gao, G.T.; Dabwan, Y.N.; Pei, G.; Dong, H. Thermal performance evaluation of subcritical organic Rankine cycle for waste heat recovery from sinter annular cooler. *J. Iron Steel Res. Int.* **2020**, *27*, 248–258. [CrossRef]
6. Shalaby, S.M.; Gadalla, M.A.; El Sayed, A.R.; Meliha, E.M.; Abosheiasha, H.F. Aspen Plus simulation of a low capacity organic Rankine cycle heated by solar energy. *Energy Rep.* **2022**, *8*, 416–421. [CrossRef]
7. Li, Y.R.; Du, M.T.; Wu, C.M.; Wu, S.Y.; Liu, C.; Xu, J.L. Economical evaluation and optimization of subcritical organic Rankine cycle based on temperature matching analysis. *Energy* **2014**, *68*, 238–247. [CrossRef]
8. Bufi, E.A.; Camporeale, S.; Fornarelli, F.; Fortunato, B.; Pantaleo, A.M.; Sorrentino, A.; Torresi, M. Parametric multi-objective optmization of an Organic Rankine Cycle with thermal energy storage for distributed generation. *Energy Procedia* **2017**, *126*, 429–436. [CrossRef]
9. Biao, M.; Zhaoliang, J.; Xianbi, L.; Yakang, F. Research progress of carbon dioxide trans-critical cycle refrigeration. *Vac. Cryog.* **2007**, *26*, 173–177.
10. Prigmore, D.; Barber, R. Cooling with the Sun's Heat Design Considerations and Test Data for a Rankine Cycle Prototype. *Sol. Energy* **1975**, *17*, 185–192. [CrossRef]
11. Jeong, J.; Kang, Y.T. Analysis of a Refrigeration Cycle Driven by Refrigerant Steam Turbine. *Int. J. Refrig.* **2004**, *27*, 33–41. [CrossRef]
12. Aphornratana, S.; Sriveerakul, T. Analysis of a Combined Rankine-Vapour-Compression Refrigeration Cycle. *Energy Convers. Manag.* **2010**, *51*, 2557–2564. [CrossRef]

13. Wu, D.; Aye, L.; Ngo, T.; Mendis, P. Optimisation and Financial Analysis of an Organic Rankine Cycle Cooling System Driven by Facade Integrated Solar Collectors. *Appl. Energy* **2017**, *185*, 172–182. [CrossRef]
14. Moloney, F.; Almatrafi, E.; Goswami, D.Y. Working fluid parametric analysis for recuperative supercritical organic Rankine cycles for medium solar reservoir temperatures. *Renew. Energy* **2020**, *147*, 2874–2881. [CrossRef]
15. Gao, H.; Liu, C.; He, C.; Xu, X.; Wu, S.; Li, Y. Performance analysis and working fluid selection of a supercritical organic Rankine cycle for low grade waste heat recovery. *Energies* **2012**, *5*, 3233–3247. [CrossRef]
16. Hu, P.; Hu, R.; Chen, Z. Working fluid selection for supercritical organic Rankine cycle. *J. Eng. Thermophys.* **2014**, *35*, 1045–1048.
17. Wang, X.; Levy, E.K.; Pan, C.; Romero, C.E.; Banerjee, A.; Rubio-Maya, C.; Pan, L. Working fluid selection for organic Rankine cycle power generation using hot produced supercritical CO_2 from a solar reservoir. *Appl. Therm. Eng.* **2019**, *149*, 1287–1304. [CrossRef]
18. Tian, H.; Shu, G.; Wei, H.; Liang, X.; Liu, L. Fluids and parameters optimization for the organic Rankine cycles (ORCs) used in exhaust heat recovery of Internal Combustion Engine (ICE). *Energy* **2012**, *47*, 125–136. [CrossRef]
19. Liang, Y.; Sun, Z.; Dong, M.; Lu, J.; Yu, Z. Investigation of a refrigeration system based on combined supercritical CO_2 power and transcritical CO_2 refrigeration cycles by waste heat recovery of engine. *Int. J. Refrig.* **2020**, *118*, 470–482. [CrossRef]
20. Sun, J.; Li, W.; Cui, B. Energy and exergy analyses of R513a as a R134a drop-in replacement in a vapor compression refrigeration system. *Int. J. Refrig.* **2020**, *112*, 348–356. [CrossRef]
21. Li, T.; Meng, N.; Liu, J.; Zhu, J.; Kong, X. Thermodynamic and economic evaluation of the organic Rankine cycle (ORC) and two-stage series organic Rankine cycle (TSORC) for flue gas heat recovery. *Energy Convers. Manag.* **2019**, *183*, 816–829. [CrossRef]
22. Turton, R.; Bailie, R.C.; Whiting, W.B.; Shaeiwitz, J.A. *Analysis, Synthesis, and Design of Chemical Processes*, 5th ed.; Pearson Education: Kraków, Poland, 2018.
23. Jenkins, S. 2019 Chemical Engineering Plant Cost Index Annual Average [EB/OL]. 2020. Available online: https://www.chemengonline.com/2019-chemical-engineering-plant-cost-index-annual-average/ (accessed on 6 March 2022).
24. Liu, S.; Li, Z.; Dai, B.; Zhong, Z.; Li, H.; Song, M.; Sun, Z. Energetic, economic and environmental analysis of air source transcritical CO_2 heat pump system for residential heating in China. *Appl. Therm. Eng.* **2019**, *148*, 1425–1439. [CrossRef]
25. Fazelpour, F.; Morosuk, T. Exergoeconomic analysis of carbon dioxide transcritical refrigeration machines. *Int. J. Refrig.* **2014**, *38*, 128–139. [CrossRef]
26. Zhao, X. *Optimal Configuration of District Cooling and Heating System Driven by Industrial Waste Heat*; Beijing University of Civil Engineering and Architecture: Beijing, China, 2019.
27. Zhou, G.Y.; Wu, E.; Tu, S.T. Optimum selection of compact heat exchangers using non-structural fuzzy decision method. *Appl. Energy* **2014**, *113*, 1801–1809. [CrossRef]